Hybrid Organic−Inorganic Quaternary Ammonium Organosilane Functionalized Mesoporous Thin Films

Eva M. Wong, Michael A. Markowitz,* Syed B. Qadri,† Stephen Golledge,‡ David G. Castner,‡ and Bruce P. Gaber

Laboratory for Molecular Interfacial Interactions, Code 6930, Center for Bio/Molecular Science and Engineering, Naval Research Laboratory, Washington, DC 20375, Surface Modification Branch, Code 6372, Materials Science and Technology Division, Naval Research Laboratory, Washington, DC 20375, and National ESCA & Surface Analysis Center for Biomedical Problems, Departments of Bioengineering and Chemical Engineering, Box 351750, University of Washington, Seattle, Washington 98195

Received: November 14, 2001

Quaternary ammonium functionalized mesoporous thin films were prepared by spin casting mixtures of bis-(triethoxysilyl)ethane hexaethoxydisilethylene with a series of quaternary ammonium functionalized organosilanes that primarily differed only in the length of the hydrocarbon segment: *N*-trimethoxysilylpropyl-*N*,*N*,*N*-trimethylammonium chloride; *N*,*N*-didecyl-*N*-methyl-(3-trimethoxysilyl-propyl)ammonium chloride; tetradecyldimethyl-(3-trimethoxysilyl-propyl)ammonium chloride; and octadecyldimethyl-(3-trimethoxysilyl-propyl)ammonium chloride. X-ray diffraction revealed that the films formed with the longest hydrocarbon segment (18 carbons) did not exhibit an ordered structure, while the remainder of the films exhibited *p6mm* pore ordering. These films remained ordered following surfactant extraction and calcination, with some film shrinkage occurring following either procedure. The *d*-spacing of the films was found to decrease linearly with increasing length of the ammonium chloride hydrocarbon segment. As determined by XPS studies, the longer hydrocarbon chain length organosilanes ($n \geq 10$) were also found to incorporate more efficiently into the films than the shorter chain material.

Introduction

Mesoporous silicate powders and thin films have been prepared and characterized by a number of research groups; however, applications using this technology are still in the nascent stages. Although powders are more straightforward to prepare in large quantities, thin films may yield advantages for sensitivity, uniformity, and transduction—characteristics that are required in sensing applications. In terms of sensing or transducing capabilities, performance of these films may be enhanced by functionalization with organic molecules and recent investigations have focused on the incorporation of a number of additives such as 3-aminopropyltriethoxysilane,[1] mercaptopropyltrimethoxysilane,[2] and tridecafluoro-1,1,2,2-tetrahydrooctyltriethoxysilane.[2] To increase the utility of films based on surface binding events or reaction sites, a porous structure is expected to allow for more rapid diffusion of species as well as to provide larger surface area leading to increased capacity and signal-to-noise ratio.

Ordered mesoporous silica thin films prepared by dip coating, spin coating, or evaporation-induced self-assembly have attracted considerable interest[3−5] for a variety of promising applications such as pH sensors,[1] chemical sensors,[6,7] mirrorless lasing,[8] and patterning.[9] Many investigations have focused strictly on the immobilization of sensing units such as enzymes,[10,11] dye molecules,[12−14] or luminescent probes.[15] Others have focused entirely on adding organic moieties by co-hydrolysis of a functional organosilane with TEOS[2,16] or integrating organic functionality via the use of bridged bistrialkoxysilanes.[17−22] However, relatively few[23,24] have investigated the additional functionality that might be gained by combining these approaches.

A simple first step toward exploring synergistic effects between bridging and pendant organic groups in thin films can be considered by co-hydrolyzing organically bridged bistrialkoxysilanes with secondary organosilanes that have terminal organic functionalities. Bridged polysilsesquioxanes can be used in sol gel applications where an organic−inorganic matrix is advantageous. The organic bridging group provides added functionality and opportunities for manipulating properties such as hydrophobicity, refractive index, chemical durability, or dielectric constant.[18] Additional modification is introduced by the cohydrolysis of a functional silane with a different organic moiety. Such a combination of organic groups could allow one to engineer a material with two or more properties; for example, enhanced hydrophobicity via the bridging group and selective adsorption by prudent choice of the secondary silane. The polysilsesquioxanes have also been widely used in the development of materials with high surface areas and controlled porosity. This combination of physical properties and chemical functionality makes them ideal candidates for catalyst supports, high capacity adsorbents, or sensing components.

Development of materials that selectively adsorb or degrade organophosphorus compounds is of significant interest because of the use of these compounds as nerve agents or pesticides.[25,26] Molecularly imprinted silica particles have been shown to selectively adsorb pinacolyl methylphosphonate (PMP), the hydrolysis product of the nerve agent soman.[27] Although

* Corresponding author. Tel: 202-404-6072. Fax: 202-767-9594. E-mail: mam@ccsalpha4.nrl.navy.mil.

† Materials Science and Technology Division, Naval Research Laboratory.

‡ University of Washington.

10.1021/jp014201g CCC: $22.00
Published on Web 06/11/2002

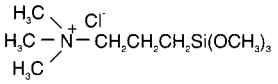

N-trimethoxysilylpropyl-*N,N,N*-trimethylammonium chloride (TMAC)

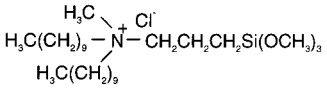

N,N-didecyl-*N*-methyl-(3-trimethoxysilylpropyl) ammonium chloride (DDMAC)

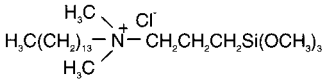

tetradecyldimethyl (3-trimethoxysilylpropyl) ammonium chloride (TDDMAC)

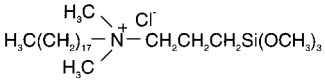

octadecyldimethyl (3-trimethoxysilylpropyl) ammonium chloride (ODDMAC)

Figure 1. Structures of quaternary ammonium functionalized organosilanes.

differences in the adsorption of PMP were observed with other organic functionalities such as pyridine and dihydroimidizole, the overall adsorption capacity increased by 2 orders of magnitude when quaternary ammonium-terminated organosilanes were incorporated into these silicate materials, suggesting a cooperative effect between the imprinted sites and the added amine functionality.[28] Extension of these qualities to a thin film is of interest for the development of surface-imprinted silicates as sensor components.

In this paper, we show the incorporation of a series of quaternary ammonium functionalized silanes to the ethane-bridged polysilsesquioxane, bis-(triethoxysilyl)ethane hexaethoxydisilethylene: *N*-trimethoxysilylpropyl-*N,N,N*-trimethylammonium chloride (TMAC), *N,N*-didecyl-*N*-methyl-(3-trimethoxysilyl-propyl)ammonium chloride (DDMAC), tetradecyldimethyl-(3-trimethoxysilyl-propyl)ammonium chloride (TDDMAC), and octadecyldimethyl-(3-trimethoxysilyl-propyl)-ammonium chloride (ODDMAC). This series of organosilanes, shown in Figure 1, was chosen to examine the effect of increasing the chain length of the hydrocarbon segments on the pore ordering, film structure, and film composition.

Experimental Section

Materials. Unless otherwise noted, all chemicals were used as received. Ethanol (reagent grade) and hydrochloric acid (reagent grade) were purchased from Aldrich Chemical Co. Pluronic P123 was purchased from BASF. Bis-(triethoxysilyl)-ethane hexaethoxydisilethylene (BTSE), *N*-trimethoxysilylpropyl-*N,N,N*-trimethylammonium chloride (TMAC, 50% solution in methanol), *N,N*-didecyl-*N*-methyl-(3-trimethoxysilyl-propyl)-ammonium chloride (DDMAC, 42% in methanol), tetradecyldimethyl-(3-trimethoxysilyl-propyl)ammonium chloride (TDDMAC, 50% in methanol), and octadecyldimethyl-(3-trimethoxysilyl-propyl)ammonium chloride (ODDMAC, 60% in methanol) were purchased from Gelest Co. Water used was deionized and distilled to 18 MΩ cm.

Film Deposition. Film solutions were prepared by stirring a mixture of 6.21 mL of ethanol and 0.259 g of P123 for 1 h and subsequently adding 0.925 mL of BTSE, 0.45 mL of H_2O, and 0.02 mL of 1 M hydrochloric acid. The functional silanes were added in the molar ratio of 1:0.025 (BTSE:XMAC) at intervals of 10, 30, and 90 min prior to spin coating. The final molar ratio of the components was 1BTSE:22EtOH:5H_2O:4 $\times$ 10^{-3} HCl:9 $\times$ 10^{-3} P123:0.025 XMAC where "X" represents the substituted (trimethoxysilyl-propyl)ammonium chloride. Films were made by filtering the solution through a 0.22 μm polyethylene filter followed by spin coating 0.4 mL of prepared solution at 2000 rpm for 30 s onto ~6.25 cm^2 sections of (100) Si wafers. All films were aged at room temperature for 2 days before extraction or calcination. Extraction was performed by placing the films in a Soxhlet extractor with refluxing ethanol for 24 h. Calcination was performed by heating the samples in air from room temperature to 100 °C at 0.5 °C/min, holding at 100 °C for 2 h, then ramping from 100 °C to 250 °C at 0.5 °C/min, and holding at 250 °C for 2 h. Control samples were processed in an identical fashion with the omission of the XMAC component.

Characterization. X-ray diffraction measurements were performed on a Rigaku Rotaflex Series model RU200B θ-2θ rotating anode diffractometer using Cu Kα radiation. Transmission electron microscopy was performed on a Hitachi H8100 TEM operating at 200 kV. Fragments of the film were scraped from the substrate and suspended in ethanol. Drops of the ultrasonicated suspension were placed onto holey carbon TEM grids. Measurements of film thickness and refractive index were made on a Gaertner L115 Waferscan model ellipsometer with an incident angle of 70°. The average and standard deviation were calculated using values taken from nine different areas of one sample. XPS was performed using a Surface Science Instrument SSX-100 spectrometer equipped with a monochromatic Al Kα X-ray source, hemispherical analyzer, and multichannel detector. Three spectra were taken for each sample, and the average and standard deviation were obtained from these data.

Results and Discussion

Thickness of the functionalized films, as determined by ellipsometry, was found to be on the order of 550−600 nm in the as-prepared condition, with shrinkage to 500−550 nm after extraction and 450 nm following calcination, whereas film thickness of the control (nonfunctionalized) films was typically 20% less in all cases, as shown in Table 1. This suggests that the addition of the quaternary ammonium silanes led to film expansion by incorporation to the matrix. Time of incorporation was found to have no effect on the film properties. In general, the film thickness was uniform over the sample area as can be inferred from the small standard deviation of less than 10%. Shrinkage of the films due to surfactant extraction was small, on the order of 5−10%, whereas contraction due to calcination was much larger, typically >25%. This can be expected since calcination may also lead to matrix densification and partial pore collapse.

As seen in Table 1, the films had refractive indices greater than 1.46 in the as-prepared condition. The incorporation of the P123 surfactant and functional silanes are the likely contributors to these larger values. In all cases, the refractive index of the films decreased upon extraction or calcination. This is the result of the elimination of the surfactant phase from the films leaving a porous structure behind. Further decreases in the refractive index with calcination may indicate that removal of the surfactant by extraction was not complete.

Although several studies have found that the incorporation of a secondary functionalized silane by the cohydrolysis route

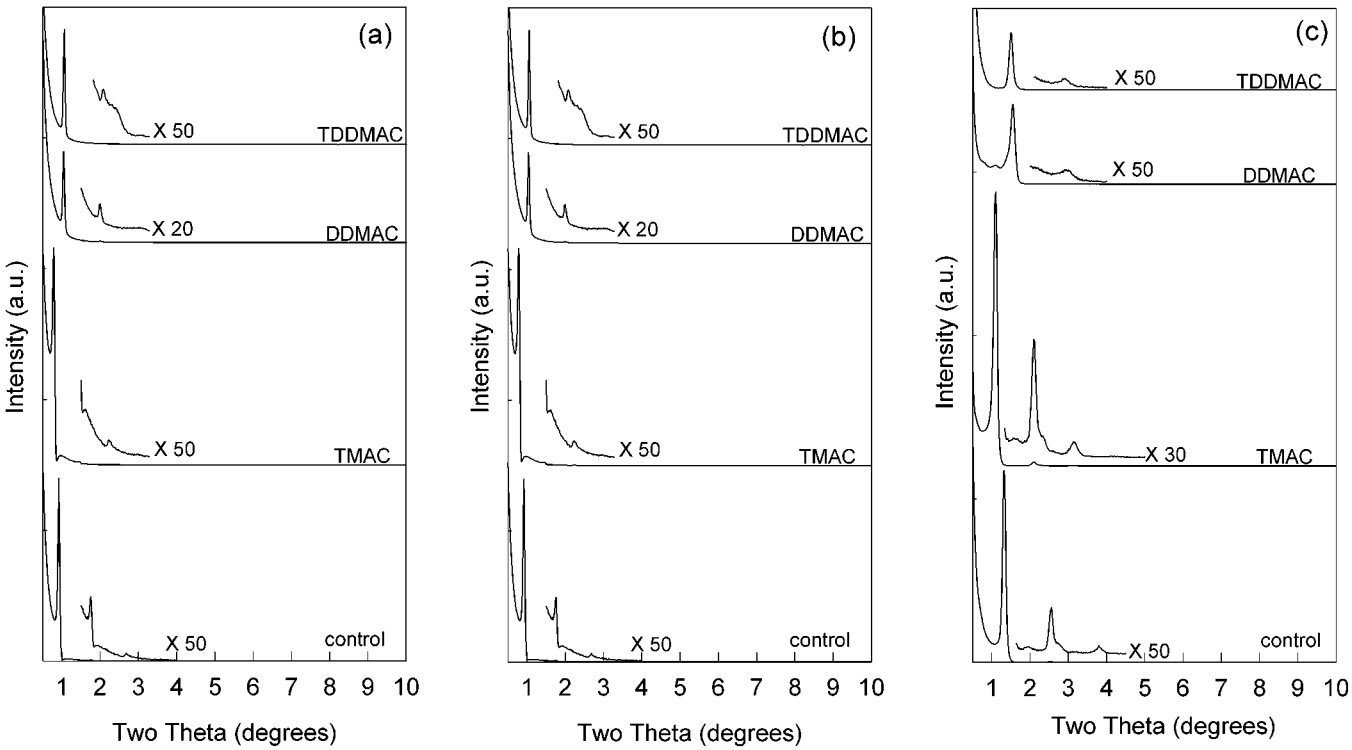

Figure 2. XRD patterns of TMAC, DDMAC, and TDDMAC functionalized films in the (a) as-prepared, (b) extracted, and (c) calcined conditions. The quaternary ammonium functionalized silanes were added 90 min prior to spin casting in the ratio of BTSE:XMAC = 1:0.025.

TABLE 1: Film Refractive Index and Thickness from Ellipsometry

	as-prepared		extracted		calcined	
silane	$\eta_{avg} \pm 3\sigma$	$t_{avg} \pm 3\sigma$ (nm)	$\eta_{avg} \pm 3\sigma$	$t_{avg} \pm 3\sigma$ (nm)	$\eta_{avg} \pm 3\sigma$	$t_{avg} \pm 3\sigma$ (nm)
Control	1.62 ± 0.19	448 ± 69	1.44 ± 0.03	383 ± 17	1.35 ± 0.14	359 ± 82
			10 min			
TMAC	1.65 ± 0.39	544 ± 91	1.35 ± 0.01	527 ± 9	1.23 ± 0.02	450 ± 24
DDMAC	1.45 ± 0.06	622 ± 22	1.29 ± 0.04	513 ± 25	1.23 ± 0.03	466 ± 11
TDDMAC	1.49 ± 0.02	625 ± 15	1.38 ± 0.04	542 ± 22	1.32 ± 0.02	461 ± 5
			30 min			
TMAC	1.60 ± 0.04	521 ± 21	1.35 ± 0.04	519 ± 64	1.25 ± 0.01	440 ± 14
DDMAC	1.54 ± 0.18	552 ± 52	1.34 ± 0.06	490 ± 44	1.23 ± 0.04	456 ± 16
TDDMAC	1.52 ± 0.04	579 ± 29	1.33 ± 0.02	553 ± 12	1.32 ± 0.01	470 ± 10
			90 min			
TMAC	2.04 ± 0.61	557 ± 94	1.33 ± 0.05	525 ± 4	1.24 ± 0.02	454 ± 26
DDMAC	1.49 ± 0.09	598 ± 74	1.25 ± 0.03	515 ± 30	1.24 ± 0.02	431 ± 54
TDDMAC	1.54 ± 0.05	559 ± 25	1.32 ± 0.02	547 ± 13	1.31 ± 0.01	472 ± 5

disrupts pore ordering,[1,2,29] with the exception of films prepared with octadecyldimethyl-(3-trimethoxysilyl-propyl)ammonium chloride (ODDMAC), all as-prepared samples were determined to have porosity ordered in two-dimensional hexagonal arrays with the long axis parallel to the substrate as indicated by the absence of (110) reflections.[30] The films prepared with ODDMAC did not show any evidence of ordering. For all other samples in the as-prepared condition, a strong (100) reflection at $2\theta = 0.78-1.06°$ and weaker (200) reflections were observed, consistent with *p6mm* type ordering. As an example, the diffraction patterns of samples with XMAC added 90 min prior to deposition are shown in Figure 2a, with the control sample shown for reference. Changes in d_{100} spacing for all samples are summarized in Table 2. Following extraction in refluxing ethanol for 24 h, the material remained hexagonally ordered, as shown in Figure 2b, and the d_{100} spacing decreased by 5−13%. Following calcination the d_{100} spacing decreased by ∼30% in all samples, however XRD patterns of the control and TMAC functionalized films revealed that the films were no longer hexagonally ordered, as shown in Figure 2c. Indexing of the X-ray diffraction patterns for the calcined control sample (d_{100} = 67 Å, d_{200} = 35 Å, d_{300} = 23 Å), and with TMAC added 90 min prior to spin coating (d_{100} = 80 Å, d_{200} = 42 Å, d_{300} = 28 Å) shows the hexagonal packing to be slightly distorted. The most likely cause of this transformation is uniaxial shrinkage of the film perpendicular to the solid silicon substrate, an effect that has also been documented in titania thin films.[31]

Although significant differences in the film thickness due to incorporation of the different quaternary ammonium silanes were not observed, changes in the d_{100} spacing were evident. The dependence of *d*-spacing on the alkyl chain length of the added functional silanes is shown in Figure 3. Here we see that by simply increasing the chain length, the *d*-spacing can be changed by over 3 nm. Addition of the TMAC has the effect of increasing the *d*-spacing compared to a control sample; however, further increasing the alkyl chain length decreases the *d*-spacing, with a near linear dependence. This relationship between hydrocarbon chain length and *d*-spacing must involve differences in the structure of the added quaternary ammonium silane. The methyl groups of these silanes are substituted with longer hydrocarbon

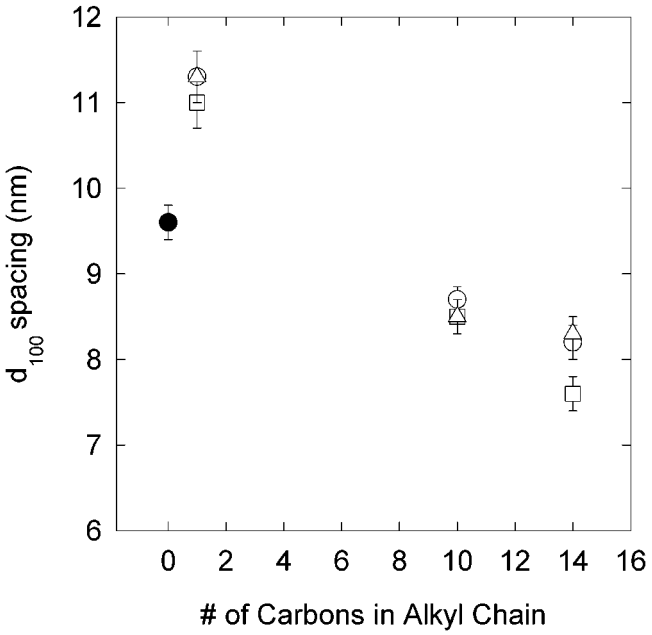

Figure 3. Dependence of *d*-spacing on length of alkyl chain backbone in as-deposited films for (●) control, functional silane added (○)10 min, (□) 30 min, and (△) 90 min prior to spin casting.

TABLE 2: Calculated Porosity, Reduction in Film Thickness, and d_{100}-Spacing Resulting from Extraction or Calcination

	chemical extraction (24 h)			calcination (250 °C/2 h)		
silane	calc. porosity (%)	Δt (%)	Δd (%)	calc. porosity (%)	Δt (%)	Δd (%)
Control	4	14.5	4.2	21	19.9	30.3
			10 min			
TMAC	21	3.1	9.3	47	17.2	29.1
DDMAC	34	17.6	8.9	47	25.1	33.8
TDDMAC	15	13.3	12.9	28	26.3	28.0
			30 min			
TMAC	21	0.4	2.4	42	45.7	29.8
DDMAC	23	11.2	5.5	47	49.1	30.7
TDDMAC	26	4.5	6.4	28	31.3	24.7
			90 min			
TMAC	26	5.7	9.3	45	48.9	29.1
DDMAC	42	14.0	8.8	45	48.7	33.3
TDDMAC	28	2.2	13.1	30	32.8	29.3

chains. Whereas the TMAC has three simple methyl groups, the DDMAC has two didecyl groups substituted for two of the methyl groups, the TDDMAC has a tetradecyl group substituted for the methyl group and for ODDMAC, an octadecyl group has been substituted for a methyl group. From the XRD, we note that although these materials had similar 2-D hexagonal structures in the as-prepared and extracted condition, seen in Figures 2a and 2b, the TMAC d_{100} peak was of significantly higher intensity. The higher-order reflections in all samples were weak, however (200) and (300) peaks were found in the TMAC functionalized material whereas only the (200) peak was found in the DDMAC and TDDMAC materials and the ODDMAC films had no detectable pore ordering. Following calcination, the TMAC and control samples retained strong ordering as evidenced by the narrow, high-intensity d_{100} peaks. The DDMAC and TDDMAC films remained ordered, but have significantly lower-intensity d_{100} peaks.

Examples of the effects of both surfactant and silane hydrocarbon chain length on silicate formation can be found in the literature. The effect of ammonium surfactant chain length on mesophase formation has been reported by Stucky[32] and the effect of the polysilsesquioxane *n*-alkylene bridging group on porosity has been reported by Shea and co-workers.[18,33,34] Shea found that with increasing alkylene bridging group length, the porosity and surface area of the fabricated xerogels decreased. Compliance of the network, which is a function of the degree of condensation at the silicon and the rigidity of the bridging group were important factors contributing to the porosity of the materials such that pore collapse could be attributed to the flexibility of the longer alkylene groups. Stucky[32] and co-workers studied quaternary ammonium surfactants of the $C_nH_{2n+1}(CH_3)_3N^+$ (C_nTMA$^+$) and $(C_{16}H_{33})(C_nH_{2n+1})N^+(CH_3)_2$ types. They found that when $n \geq 20$ in the alkyltrimethylammonium surfactants, low-surface curvature mesophases formed leading to the formation of lamellar silicate phases. Shorter chain surfactants were found to give MCM-41. Furthermore, when $n > 4$ the substituted surfactants were found to behave more like surfactants with two identical alkyl chains. It was hypothesized that the substituted group is too long and hydrophobic to remain fully exposed to the water region as part of the headgroup. The structures varied from MCM-41 to MCM-50 with increasing *n*, and were accompanied by decreasing *d*-spacing.

The differences in the observed properties between the shorter alkyl chain TMAC and longer alkyl chain DDMAC and TDDMAC materials may be explained by considering the previous discussion. One possible reason for the observed dependence of *d*-spacing on hydrocarbon chain length may be that the longer dodecyl, tetradecyl, and octadecyl segments are more flexible than the TMAC methyl segment allowing bending or coiling to occur thereby disrupting the local environment. Indeed, the significantly longer octadecyl segment was found to interrupt the structure to the extent that pore ordering was entirely absent.

Changes in the d_{100} spacing due to post formation processes, extraction, and calcination, were also evident. Extraction yielded only small changes in the d_{100} spacing (typically less than 15% reduction), indicating that the pore ordering and spacing remained intact when the surfactant was removed from the matrix. Changes in the d_{100} spacing were much more dramatic following calcination due to large decreases in the film thickness and pore contraction. Despite this film shrinkage and reduction in pore spacing, the films remained well ordered as demonstrated by the XRD patterns shown in Figure 2.

The structure of the films was examined using transmission electron microscopy. Representative micrographs of a functionalized film are shown in Figure 4. A cross section of an extracted film prepared with TMAC added 90 min prior to deposition film is shown in Figure 4a. The lighter contrast area represents the pore space and the darker contrast area represents the matrix material. From this image one can observe that the pores are ordered with a *d*-spacing of 10.5 nm, $a_0 = 12$ nm, pore diameter of 5−6 nm, and wall thickness of ∼6 nm. A cross section from the same film showing the long axis of pores is presented in Figure 4b. Again, regular spacing of the pores is seen. The diameter of the pores shown here is ∼6 nm with wall thickness of ∼5 nm. The measurements taken from Figure 4b correspond with the information gathered from the view in Figure 4a indicating that the material is well ordered with uniform properties.

The effect of calcination on pore structure was observed in the nonfunctionalized film (control) as shown in Figure 5. Figure 5a shows pore ordering with *d*-spacing of ∼6.5 nm and wall thickness of ∼5−6 nm. In this image, contraction of the pores in one dimension is evident from the shape of the pores where

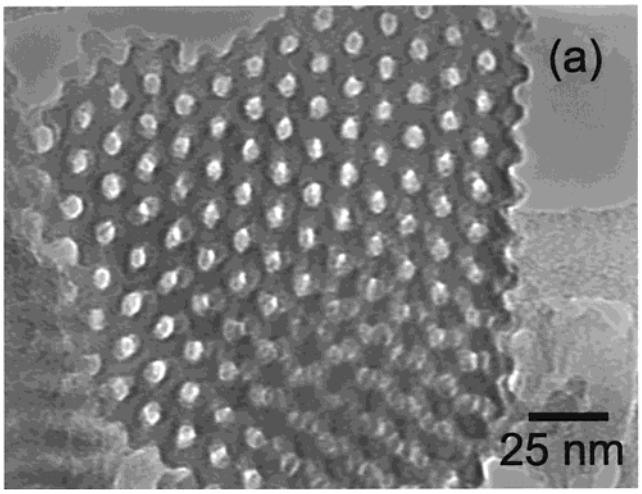

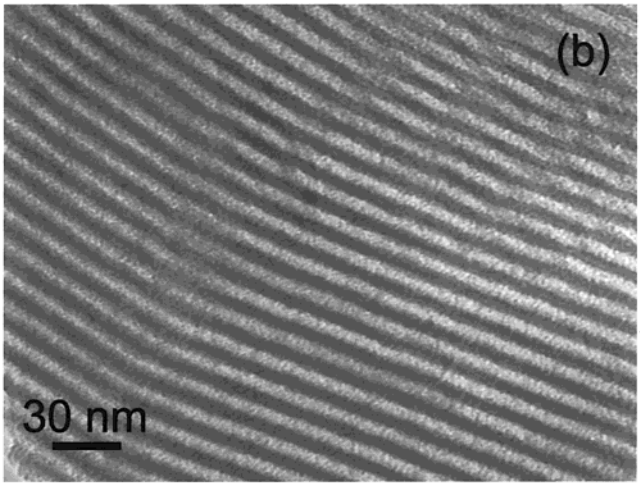

Figure 4. TEM images of an extracted film prepared with TMAC added 90 min prior to deposition. (a) Cross section of film showing pore ordering with a *d*-spacing of 10.5 nm, $a_0 = 12$ nm, and pore diameter of 5−6 nm. (b) Cross section of different area from the same film showing long axis of pores with regular spacing and pore diameter of 6 nm and a wall thickness of ∼5 nm.

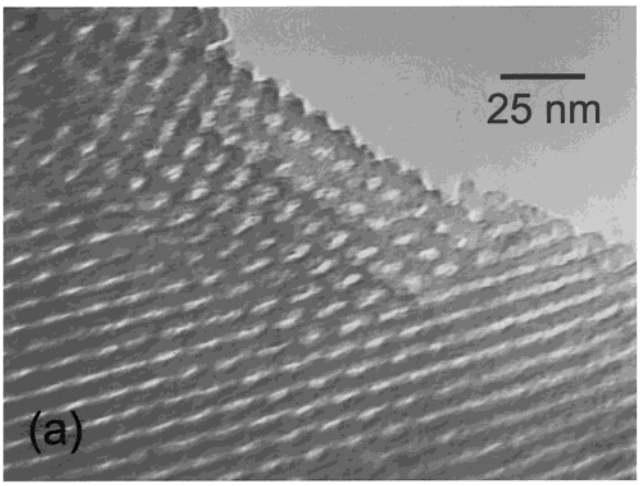

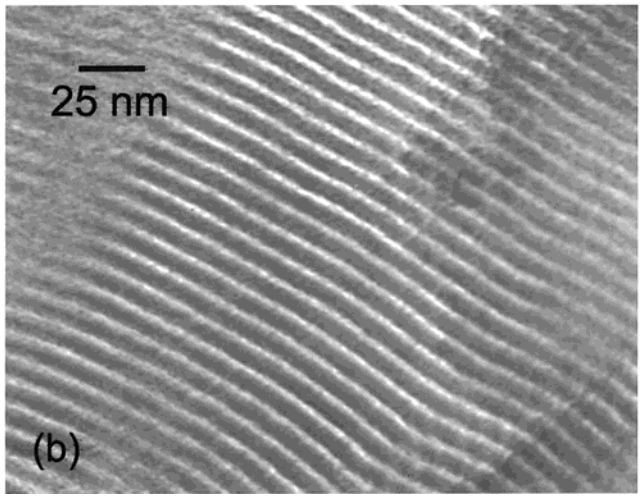

Figure 5. TEM images of a nonfunctionalized calcined film. (a) Cross section of film showing pore ordering and contraction with a *d*-spacing of ∼6.5 nm and pore diameter of 2−3 nm. (b) Cross section of different area from the same film showing long axis of pores with regular spacing and pore diameter of 3 nm and a wall thickness of ∼5 nm.

the pore diameter is 2−3 nm in one direction and 5−6 nm in the other. This contraction of the pore structure can also be seen in a cross section from the same film (Figure 5b), showing the long axis of the pores. Regular spacing of the pores is observed with pore diameter of ∼2.5 nm and wall thickness of ∼6 nm.

The observed nonuniform contraction of the films is attributed to the unidirectional shrinkage of the films during calcination. Since the films are deposited onto Si wafers, the relatively rigid substrate limits film contraction parallel to the film surface, whereas shrinkage perpendicular to the film substrate is unrestricted. This uniaxial shrinkage can also give rise to a change in pore ordering as evidenced by the XRD patterns of the calcined nonfunctionalized and TMAC functionalized films.

Porosity measurements of mesoporous thin films have been somewhat limited due to the difficulty in using standard nitrogen adsorption equipment to measure the limited sample mass associated with thin films. Alternative approaches to performing porosity measurements of silicate thin films have been reported by a number of groups using several techniques such as SAW devices,[35,36] positronium annihilation,[37] ellipsometric porosimetry,[38] ellipsometry,[39] and X-ray reflectivity density measurements.[40] Of these, SAW combined with porosimetry is probably the most accurate; however, ellipsometry calculations are the most straightforward, although many assumptions must be made. Taylor obtained very good results when the porosity of porous silica measured by porosimetry was compared to that obtained by ellipsometry.[39] A simple calculation can be made to estimate the porosity of the extracted and calcined films from the refractive indices using the Lorentz−Lorenz relation:[41]

$$\left(\frac{\eta_f^2 - 1}{\eta_f^2 + 2}\right) = (1 - \nu_p)\left(\frac{\eta_s^2 - 1}{\eta_s^2 + 2}\right) + \nu_p\left(\frac{\eta_p^2 - 1}{\eta_p^2 + 2}\right) \qquad (1)$$

where ν_p is the fraction of porous phase, η_p is the refractive index of the material in the pores, η_s is the refractive index of the solid matrix material at theoretical density, and η_f is the measured refractive index of the film. In the dry state the pores can be assumed to be filled with air, which has a refractive index of unity, such that the porous fraction can be rewritten as

$$\nu_p = 1 - \left[\left(\frac{\eta_f^2 - 1}{\eta_f^2 + 2}\right)\left(\frac{\eta_s^2 + 2}{\eta_s^2 - 1}\right)\right] \qquad (2)$$

Although the film matrixes contained incorporated alkyl and amine groups and therefore were not pure SiO_2, to a first approximation the refractive index of SiO_2 at 100% theoretical density, $\eta_s = 1.46$, may be used. Given the assumptions made,

TABLE 3: Concentration of All Measured Species by XPS, Given in Atomic Percent

sample	C	O	N	Si	Cl
		As-Prepared			
Control	49.7 ± 0.6	36.5 ± 1.0		13.8 ± 0.5	
TMAC	48.1 ± 1.6	35.9 ± 0.6	0.5 ± 0.1	15.0 ± 1.1	0.5 ± 0.1
TDDMAC	61.5 ± 0.2	23.1 ± 0.2	1.8 ± 0.1	11.7 ± 0.3	2.0 ± 0.1
DDMAC	67.4 ± 0.5	18.7 ± 0.2	1.8 ± 0.1	10.1 ± 0.4	2.0 ± 0.2
		Extracted			
Control	39.5 ± 0.6	39.7 ± 0.2		20.8 ± 0.7	
TMAC	37.9 ± 0.8	38.3 ± 0.5	0.6 ± 0.1	22.7 ± 0.6	0.5 ± 0.1
TDDMAC	50.0 ± 0.2	30.3 ± 0.5	1.2 ± 0.2	17.7 ± 0.1	0.8 ± 0.1
DDMAC	56.4 ± 2.0	25.2 ± 0.7	1.6 ± 0.8	15.7 ± 0.4	1.0 ± 0.4
		Calcined			
Control	23.2 ± 0.6	49.7 ± 0.2		27.3 ± 0.3	
TMAC	25.4 ± 1.6	48.3 ± 0.8	0.3 ± 0.3	26.0 ± 0.9	
TDDMAC	25.7 ± 1.1	50.6 ± 0.9	0.6 ± 0.1	23.2 ± 0.4	
DDMAC	20.1 ± 0.7	52.5 ± 0.2		27.4 ± 0.8	

TABLE 4: Measured N/Si Ratio Obtained from XPS and Calculated % Incorporation of XMAC (shown in parentheses)

	as-prepared	extracted	calcined
TMAC	0.033 ± 0.009 (70 ± 20%)	0.026 ± 0.005 (56 ± 10%)	0.014 ± 0.010 (29 ± 21%)
DDMAC	0.178 ± 0.016 (374 ± 34%)	0.102 ± 0.052 (214 ± 110%)	
TDDMAC	0.154 ± 0.012 (323 ± 25%)	0.068 ± 0.012 (142 ± 25%)	0.026 ± 0.005 (54 ± 10%)

the porosity values are expected to be very approximate, however they do indicate that the average porosity for extracted samples was on the order of 20−35% and 30−45% following calcination, as summarized in Table 2. Functionalization of the BTSE seems to have increased the porosity of the film. This may occur by expanding the pore diameter by functionalization at the pore surface.

XPS of films prepared by adding 2.5 mol % XMAC (relative to BTSE) 90 min prior to deposition was performed to measure the relative C, O, N, Cl, and Si content. The concentration of all measured species is shown in Table 3. The ratio of nitrogen to silicon was used to calculate the percentage of XMAC that was incorporated into the films by comparing to the amount added to the solution. Both the measured N/Si ratio and the calculated percentage incorporation of TMAC are shown in Table 4. As expected, nitrogen was not detected in the control samples. Significant drops in nitrogen concentration as a result of extraction and calcination procedures were observed in all samples. Chloride initially bound to the nitrogen in the as-prepared and extracted condition was removed following calcination, suggesting that an exchange reaction may have occurred with OH^- during the high-temperature process. Lower concentrations of functional silane in the extracted and calcined products indicate that a portion of the functional silanes is removed during extraction or calcination.

Incorporation of TMAC was on the order of 70% in the as-prepared condition and decreased to 56% following extraction. Calculated TDDMAC and DDMAC incorporation into the films was noticeably higher than the amount of organosilane initially added to the solution. Previous reports have shown similar results for the incorporation of trialkoxy organosilanes with thiol, amine, epoxide, imidazole, or allyl functionalities into mesoporous silica.[42] Increased concentration of the functionalized silane in the film relative to the initial mixture may be attributed to differing rates of hydrolysis and condensation for the matrix precursor (BTSE) and organosilane. From the XPS results, we note that the tetradecyl-dimethyl-*N*-propyl and *N*,*N*-didecyl-*N*-methyl-*N*-propylammonium groups were incorporated more efficiently than the trimethyl-*N*-propylammonium group.

One explanation may be that these organosilanes may hydrolyze more rapidly when compared to the stable BTSE precursor or even self-condense.[24] In a study by Hook[43] of the sol−gel polymerization rates of substituted ethoxysilanes, the hydrolysis and condensation rates of four alkyl (hydro, methyl, ethyl, vinyl)-substituted triethoxysilanes were examined. Ethyl- and hydro-substituted silanes were found to undergo hydrolysis at a rate which was an order of magnitude faster than that of the methyl- and vinyl-substituted silanes and likewise the initial condensation rates of the ethyl- and hydro-substituted silanes was 15 and 45 times greater than the methyl-substituted ethoxysilane. The vinyl group is expected to slow reaction compared to the methyl group due to its weak electron withdrawing ability and the hydro group is favorable for steric reasons. Since the resonance and inductive effects of the ethyl and methyl groups can be expected to be very similar, the faster hydrolysis rates of the ethyl group over the methyl group were explained by considering the polarizability constant, σ_α. The polarizability is dependent on size and number of electrons present and how tightly they are controlled by the nucleus such that groups with high polarizability can set up a dipole which stabilizes a charged molecule. Since the polarizability of the ethyl group ($\sigma_\alpha = 0.49$) is larger than the methyl group ($\sigma_\alpha = 0.35$), protonation is increased thereby leading to increased hydrolysis. The seemingly small change made by substituting an ethyl for a methyl group clearly made large differences in the gelation behavior of the triethoxysilanes. While the substituted trimethoxysilyl-propylammonium chlorides studied here are not simple analogues to the substituted silanes studied by Hook,[43] the observed differences in incorporation between the TMAC, and longer alkyl chain DDMAC and TDDMAC may stem from differences in polarizability leading to differing hydrolysis and condensation rates. Further studies using ^{29}Si NMR could be expected to elucidate the effects of the alkyl chain length and polarizability of the specific organosilanes studied on incorporation efficiency.

A second explanation for this may be found by considering that the XPS composition data is obtained from the outer 5 nm of the film, thus the XPS surface composition may be significantly different from the overall film composition. N/Si ratios higher than the expected value then could be due to surface enrichment of the nitrogen-containing silane. The increased size of the TDDMAC and DDMAC silane may impose steric constraints such that these silanes would be preferentially bound to the outer surface of the film rather than inside the pore surface. Further studies addressing the possibility of surface enrichment are planned.

Conclusions

Our results indicate that functionalized quaternary ammonium organosilanes can be successfully incorporated into ordered organic−inorganic silica mesophases by co-condensation reactions in the presence of surfactant templates. The 2-D hexagonal, *p6mm* type ordered pore structure was maintained following extraction as determined by TEM and XRD. Following calcination at 250 °C, the nonfunctionalized and TMAC functionalized materials were found to exhibit 2-D cubic pore ordering, which likely resulted from nonuniform film shrinkage and partial pore collapse. Based on compositional data obtained from XPS, *N*,*N*-didecyl-*N*-methyl-(3-trimethoxysilyl-propyl)ammonium chloride and tetradecyldimethyl-(3-trimethoxysilyl-propyl)ammonium chloride were incorporated more efficiently than the *N*-tri-

methoxysilylpropyl-*N*,*N*,*N*-trimethylammonium chloride. From XRD, the incorporated trimethyl-*N*-propylammonium group led to an increase in the *d*-spacing of the pores relative to the matrix prepared without added ammonium functionality whereas the tetradecyldimethyl-*N*-propyl and *N*,*N*-didecyl-*N*-methyl-*N*-propylammonium groups decreased the *d*-spacing. These results demonstrate that the length of the hydrocarbon segment of the quaternary ammonium functionalized silanes has a significant effect on the properties of the formed films. These films are expected to offer opportunities for molecular imprinting and selective binding of organophosphonate complexes.

Acknowledgment. E. M. Wong is a National Research Council Postdoctoral Research Associate at the Naval Research Laboratory. This project was funded by the Office of Naval Research through a Naval Research Laboratory Accelerated Research Initiative and the Joint Service CB Defense Technology Base Program. The National ESCA & Surface Analysis Center for Biomedical Problems at the University of Washington is a NIH-supported research center, RR-01296.

References and Notes

(1) Wirnsberger, G.; Scott, B. J.; Stucky, G. D. *Chem. Commun.* **2001**, 119.
(2) Fan, H.; Lu, Y.; Stump, A.; Reed, S. T.; Baer, T.; Schunk, R.; Perez-Luna, V.; Lopez, G. P.; Brinker, C. J. *Nature* **2000**, *405*, 56.
(3) Scott, B. J.; Wirnsberger, G.; Stucky, G. D. *Chem. Mater*. **2001**, *13*, 3140.
(4) Edler, K. J.; Roser, S. J. *Int. Rev. Phys. Chem.* **2001**, *20*, 387.
(5) Pevzner, S.; Regev, O.; Yerushalmi-Rozen, R. *Curr. Opin. Colloid Interface Sci*. **2000**, *4*, 420.
(6) Innocenzi, P.; Martucci, A.; Guglielmi, M.; Bearzotti, A.; Traversa, E.; Pivin, J. C. J. *Eur. Ceram. Soc.* **2001**, *21*, 1985.
(7) Domansky, K.; Liu, J.; Wang, L.-Q.; Engelhard, M. H.; Baskaran, S. *J. Mater. Res*. **2001**, *16*, 2810.
(8) Yang, P.; Wirnsberger, G.; Huang, H. C.; Cordero, S. R.; McGehee, M. D.; Scott, B.; Deng, T.; Whitesides, G. M.; Chmelka, B. F.; Buratto, S. K.; Stucky, G. D. *Science* **2000**, *287*, 465.
(9) Doshi, D. A.; Huesing, N. K.; Lu, M.; Fan, H.; Lu, Y.; Simmons-Potter, K.; Potter, B. G.; Hurd, A. J.; Brinker, C. J. *Science* **2000**, *290*, 107.
(10) Yiu, H.; Wright, P. A.; Botting, N. P. *Microporous Mesoporous Mater.* **2001**, *44*, 763.
(11) Takahashi, H.; Li, B.; Sasaki, T.; Miyazaki, C.; Kajino, T.; Inagaki, S. *Microporous Mesoporous Mater.* **2001**, *44*, 755.
(12) Honma, I.; Zhou, H. S. *Adv. Mater*. **1998**, *10*, 1532.
(13) Ogawa, M.; Ishikawa, H.; Kikuchi, T. *J. Mater. Chem*. **1998**, *8*, 1783.
(14) Lebeau, B.; Fowler, C. E.; Hall, S. R.; Mann, S. *J. Mater. Chem*. **1999**, *9*, 2279.
(15) Hernandez, R.; Franville, A.-C.; Minoofar, P.; Dunn, B.; Zink, J. I. *J. Am. Chem. Soc*. **2001**, *123*, 1248.
(16) Dag, O.; Yoshina-Ishii, C.; Asefa, T.; MacLachlan, M. J.; Grondey, H.; Coombs, N.; Ozin, G. A. *Adv. Funct. Mater*. **2001**, *11*, 213.
(17) Lu, Y.; Fan, H.; Doke, N.; Loy, D. A.; Assink, R. A.; LaVan, D. A.; Brinker, C. J. *J. Am. Chem. Soc*. **2000**, *122*, 5258.
(18) Shea, K. J.; Loy, D. A. *Chem. Mater*. **2001**, *13*, 3306.
(19) Cho, E. B.; Kwon, K. W.; Char, K. *Chem. Mater*. **2001**, *13*, 3837.
(20) Asefa, T.; Kruk, M.; MacLachlan, M. J.; Coombs, N.; Grondey, H.; Jaroniec, M.; Ozin, G. A. *J. Am. Chem. Soc*. **2001**, *123*, 8520.
(21) Stein, A.; Melde, B. J.; Schroden, R. C. *Adv. Mater*. **2000**, *12*, 1403.
(22) Kruk, M.; Jaroniec, M.; Guan, S. Y.; Inagaki, S. *J. Phys. Chem. B* **2001**, *105*, 681.
(23) Calleja, G.; Cerveau, G.; Corriu, R. J. P. *J. Organomet. Chem.* **2001**, *621*, 46.
(24) Burleigh, M. C.; Markowitz, M. A.; Spector, M. S.; Gaber, B. P. *J. Phys. Chem. B* **2001**, *105*, 9935.
(25) Yang, Y. C. *Acc. Chem. Res*. **1999**, *32*, 109.
(26) Kanan, S. M.; Tripp, C. P. *Langmuir* **2001**, *7*, 2213.
(27) Markowitz, M. A.; Deng, G.; Gaber, B. P. *Langmuir* **2000**, *16*, 6148.
(28) Markowitz, M. A.; Deng, G.; Burleigh, M. C.; Wong, E. M.; Gaber, B. P. *Langmuir* **2001**, *17*, 7085.
(29) Hall, S. R.; Fowler, C. E.; Lebeau, B.; Mann, S. *Chem. Commun*. **1999**, 201.
(30) Zhao, D.; Yang, P.; Melosh, N.; Feng, J.; Chmelka, B. F.; Stucky, G. D. *Adv. Mater*. **1998**, *10*, 1230.
(31) Grosso, D.; Soler-Illia, G. J.; Babonneau, F.; Sanchez, C.; Albouy, P.-A.; Brunet-Bruneau, A.; Balkenende, A. R. *Adv. Mater*. **2001**, *12*, 1085.
(32) Huo, Q.; Margolese, D. I.; Stucky, G. D. *Chem. Mater*. **1996**, *8*, 1147.
(33) Oviatt, H. W.; Shea, K. J.; Small, J. H. *Chem. Mater*. **1993**, *5*, 943.
(34) Loy, D. A.; Jamison, G. M.; Baugher, B. M.; Russick, E. M.; Assink, R. A.; Prabakar, S.; Shea, K. J. *J. Non-Cryst. Solids* **1995**, *186*, 44.
(35) Hietala, S. L.; Smith, D. M. *Langmuir* **1992**, *9*, 249.
(36) Frye, G. C.; Ricco, A. J.; Martin, S. J.; Brinker, C. J. In *Better Ceramics Through Chemistry III*; Brinker, C. J., Clark, D. E., Ulrich, D. R., Eds.; Materials Research Society: Pittsburgh, 1998; Vol. 121, p 349.
(37) Dull, T. L.; Frieze, W. E.; Gidley, D. W.; Sun, J. N.; Yee, A. F. *J. Phys. Chem. B* **2001**, *105*, 4657.
(38) Baklanov, M. R.; Mogilnikov, K. P.; Polovinkin, V. G.; Dultsev, F. N. *J. Vac. Sci. Technol. B* **2000**, *18*, 1385.
(39) Taylor, D. J.; Fleig, P. F.; Hietala, S. L. *Thin Solid Films* **1998**, *322*, 257.
(40) Windover, D.; Lum, T.-M.; Lee, S. L.; Kumar, A.; Bakhru, H.; Jin, C.; Lee, W.; *Appl. Phys. Lett*. **2000**, *76*, 158.
(41) Born, M.; Wolf, E. *Principles of Optics*, 4th ed.; Pergamon Press: Oxford, 1970; Chapter 2.
(42) Fowler, C. E.; Burkett, S. L.; Mann, S. *Chem. Commun*. **1997**, 1769.
(43) Hook, R. J. *J. Non-Cryst. Solids* **1996**, *195*, 1.